Dalton Transactions

ROYAL SOCIETY OF CHEMISTRY

PAPER

View Article Online
View Journal | View Issue

Cite this: *Dalton Trans.*, 2024, **53**, 15551

Multinuclear beryllium amide and imide complexes: structure, properties and bonding†

Deniz F. Bekiş, ‡ Lewis R. Thomas-Hargreaves,‡ Sergei I. Ivlev and Magnus R. Buchner *

Received 8th August 2024,
Accepted 26th August 2024

DOI: 10.1039/d4dt02269f

rsc.li/dalton

The beryllium amide and imide complexes $[Be(HNMes)_2]_3$, $[(py)_2Be(HNMes)_2]$, $[Be(HNDipp)_2]_2$, $[Be(NPh_2)(\mu_2\text{-}HNDipp)]_2$ and $[Be(NCPh_2)_2]_3$ have been prepared and characterised with NMR and IR spectroscopy as well as single crystal X-ray diffraction. Analysis of the localised molecular orbitals (LMOs) and intrinsic atomic orbital (IAO) atomic charges in the framework of the intrinsic bond orbital (IBO) localization method revealed a covalent bonding network consisting of 2-electron–2-centre and 2-electron–3-centre σ bonds, in which one electron pair of the anionic N-donor ligands is involved. The electron deficiency at the beryllium atoms is partially compensated through additional electron donation from the lone pair at the nitrogen atoms.

1 Introduction

The chemistry of low valent s-block and early p-block metals has received a lot of attention in the last two decades.[1–4] Most of these low valent compounds were isolated utilising N-donor ligands.[5–8] This is not the case, however, for the lightest group 2 metal, beryllium, of which low valent compounds have, with one exception,[9] only been realised with C-donor ligands.[10–16] There are only few described reductions of N-donor complexes of beryllium, which resulted in the formation of beryllates.[17–19] Considering the huge number of beryllium complexes with N-donor ligands that have been recently published,[20–35] it can be assumed that reduction attempts have been performed on some of these systems but did not yield defined compounds. Furthermore, no generally applicable reducing agent to obtain low valent beryllium has been found yet, and each ligand system requires special reduction conditions.[10–16] Therefore, it is evident that too little is known about the properties of beryllium compounds to rationally select ligands and reducing agents. For this reason we have been studying simple beryllium halide complexes and organoberyllium compounds extensively.[36–44]

Considering the abundance of N-donor complexes in main group metal chemistry, it is no surprise that there are many reports on heteroleptic organo beryllium amines, amides and some imides of the types $(R_3N)BeX_2$ (X = Cl, Br, I),[54,55] $[(R_2N)BeR']_n$ [56–59] and $[(R_2C{=}N)BeR']_n$, respectively.[60] However, there are only few described homoleptic beryllium N-donor compounds. To the best of our knowledge $[Be(NH_3)_4]^{2+}$ (**I**, Fig. 1)[45,46] and $[Be(py)_4]^{2+}$ [61] are the only homoleptic beryllium compounds in which the metal is only coordinated by amines. In homoleptic beryllium amides, the coordination number of the central atom varies. In $[Be(N(SiMe_3)_2)_2]$ (**II**) the beryllium atom is dicoordinated,[47–50] and the Be–N bond exhibits partial double bond character.[50] Similar bonding has also been described in a beryllium imido complex.[62] Reaction of $BeCl_2$ with dialkyl amines and subsequent treatment with organo-

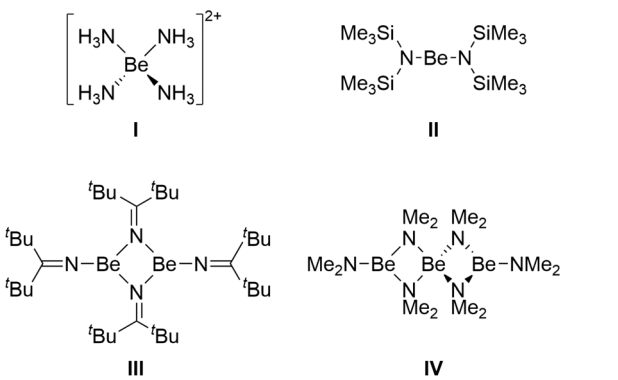

Fig. 1 Structurally authenticated mono-, di- and trinuclear beryllium complexes with N-donor ligands.[45–53]

Anorganische Chemie, Nachwuchsgruppe Hauptgruppenmetallchemie, Fachbereich Chemie, Philipps-Universität Marburg, Hans-Meerwein-Straße 4, 35032 Marburg, Germany. E-mail: magnus.buchner@chemie.uni-marburg.de; Fax: +49 (0)64212825669; Tel: +49 (0)6421 2825668

†Electronic supplementary information (ESI) available: Extended crystallographic data, IR and NMR spectra. CCDC 2373010–2373014. For ESI and crystallographic data in CIF or other electronic format see DOI: https://doi.org/10.1039/d4dt02269f

‡Equal author contribution.

lithium compounds gives homoleptic $[Be(NR_2)_2]_{1-3}$, which are described as mono-, di- and trimeric in solution.[63] $[Be(N^iPr_2)_2]_{1-2}$ is described to be isolatable as a mono- and a dimeric isomer, however their reactivity with CS_2 is identical.[64] With a sterically demanding imide dinuclear $[Be(N{=}C^tBu_2)_2]_2$ (**III**) was obtained and its structure and spectroscopic properties investigated,[51,52] while utilisation of small dimethylamide results in the formation of trinuclear $[Be(NMe_2)_2]_3$ (**IV**).[53]

Due to the large variety of the ligands in these homoleptic amide and imide complexes, no clear trends concerning the influence of electronic and steric properties of the ligands onto the constitution of the respective beryllium complexes can be derived. However, this knowledge is the first step for a rational design of beryllium complexes with N-donor ligands. Therefore, we prepared beryllium compounds with selected amido and imido ligands, to investigate their electronic and steric influence on the structure and spectroscopic properties of the derived complexes.

2 Results and discussion

For the synthesis of the desired beryllium amides, direct deprotonation of amines with beryllium organic compounds was chosen. This approach had already been established by Coates *et al.*[57] Addition of 2,4,6-trimethylaniline (H_2NMes) to a benzene solution of $BeEt_2$ resulted in immediate gas evolution. However, full conversion could only be achieved by heating the reaction solution to 70 °C for 20 h. Even though this reaction is quantitative according to NMR spectroscopy, homoleptic beryllium amide $[Be(HNMes)_2]_3$ (**1**) could only be isolated in a moderate yield of 64% (Fig. 2). **1** is well soluble in benzene and crystals suitable for single crystals X-ray diffraction analysis could be obtained by slow solvent evaporation.

1 crystallises in the triclinic space group $P\bar{1}$ (2) with two formula units per unit cell. The trinuclear compound comprises one central beryllium atom, which is connected to two terminal beryllium atoms *via* two μ_2-bridging amido nitrogen atoms, each. The coordination sphere of the terminal beryllium atoms is completed by an additional amido ligand. This results in a linear trinuclear beryllium amide, in which the central beryllium atom is tetra-coordinated while the terminal beryllium atoms are only tri-coordinated, as depicted in Fig. 3. This structural motif is known from $[Be(NMe_2)_2]_3$,[53] $[BePh_2]_3$ [40] and $[Be(O_2{}^tBu)]_3$.[65] The molecules of **1** are heavily disordered in the crystal, which leads to a huge variation in bond lengths and angles. The Be–Be–Be angle in **1** is with 170.8(4)–174.9(5)° close to the one in $[Be(O_2{}^tBu)]_3$ (175.5(2)°),[65] slightly smaller than in $[Be(NMe_2)_2]_3$ (179.985°)[53] and significantly larger than in $[BePh_2]_3$ (141.72(8)°).[40] The Be···Be distance in **1** is with 2.247(11)–2.379(9) Å comparable to $[Be(NMe_2)_2]_3$ (2.300(9) Å)[53] and $[Be(O_2{}^tBu)]_3$ (2.2836(17) Å),[65] which is considerably above the sum of the single bond covalent radii of beryllium (1.02 Å).[66] It should be noted that the Be···Be separations in $[BePh_2]_3$ (2.033(2) & 2.047(2) Å) are considerably shorter than in **1**.[40] The Be–N bonds to the central beryllium atom are with 1.756(3)–1.768(3) Å longer than those of the terminal beryllium atoms to the non-bridging amido ligands (1.540(11)–1.604(9) Å), while the atom separations of the terminal beryllium atoms to the bridging nitrogen atoms are due to their huge variation (1.482(13)–1.885(9) Å) identical to the other Be–N bond lengths in **1**. These atomic separations compare well to those found in $[Be(NMe_2)_2]_3$ (Be2–N_μ 1.653(7) Å, Be1/3–N1/6 1.573(11) Å, Be1/3–N_μ 1.785(4) Å; labelling scheme in analogy to Fig. 3)[53] and are by tendency shorter than in related heteroleptic compounds.[65,67] While the bridging nitrogen atoms are pseudo-tetrahedrally coordinated, the terminal nitrogen atoms

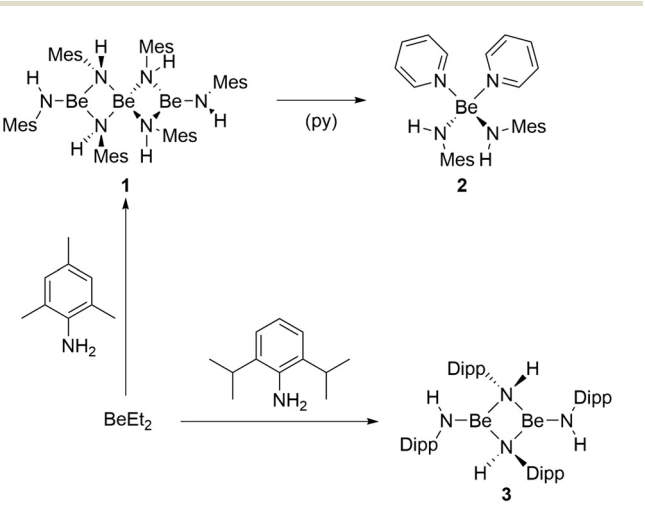

Fig. 2 Reaction of diethyl beryllium with 2,4,6-trimethylaniline (H_2NMes) or 2,6-diisopropylaniline (H_2NDipp).

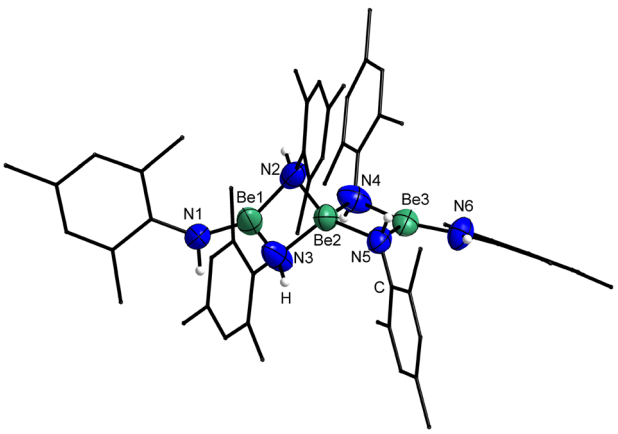

Fig. 3 Solid state structure of **1**. Ellipsoids are depicted at 70% probability at 100 K, while hydrogen atoms are shown isotropic with arbitrary radii. Carbon bound hydrogen atoms are omitted and carbon atoms shown as wire-frame for clarity. Selected bond lengths (Å) and angles (°): Be···Be 2.247(11)–2.379(9), Be1/3–N_μ 1.482(13)–1.885(9), Be2–N_μ 1.756(3)–1.768(3), Be1/3–N1/6 1.540(11)–1.604(9); Be1/3–N_μ–Be2 78.0(4)–90.7(4), N_μ–Be2–N_μ 92.7(1)–118.6(2), N_μ–Be1/3–N_μ 94.9(4)–101.5(6), N1/6–Be1/3–N_μ 111.1(8)–146.6(8), N1/6–Be1/3–Be2 162.8(9)–167.1(7), Be1–Be2–Be3 170.8(4)–174.9(5), N1/6–Be1/3–N_μ–Be2 173.8(19)–179.7(6); angle between Be1/3N_3 planes: 89.2(2)–89.9(2)°.

exhibit a planar coordination sphere. To evaluate this unexpected structural feature and to understand the bonding situation in **1**, localised molecular orbital (LMO) and intrinsic atomic orbital (IAO) atomic charge analysis was performed.[68,69]

All structures of non-deprotonated ligands and complexes were optimized at the DFT-PBE0/def2-TZVP level of theory, and the resulting bond lengths and angles in the gas-phase are in good agreement with the experimental results. Therefore, the applied computational model can confidently be used for bonding analysis. On the basis of the obtained Kohn–Sham DFT wave functions, LMOs and IAO atomic charges were obtained by using the intrinsic bond orbital (IBO) localization method.[68] The IAO atomic charges of the beryllium atoms in **1** are 1.48 to 1.51, while those at the nitrogen atoms range from −0.96 to −1.03 (ESI Fig. S27†). These charges are in line with the electronegativity difference of the two bonding partners. Comparison of the deprotonated ligand in **1** and free H_2NMes (ESI Fig. S28†) shows increased negative charge at the nitrogen atoms in the deprotonated coordinated ligand, as would be expected. While the charge at the carbon atom bound to the nitrogen atom of the terminal amido ligands is not significantly different to the one calculated for free H_2NMes, this carbon charge is significantly reduced in the bridging amido ligands. Additionally, the charge of the bridging nitrogen atoms is significantly more negative than in their terminal counterparts. LMO analysis of **1** reveals two sets of bonds between the terminal beryllium atoms and the non-bridging nitrogen atoms as depicted in Fig. 4(a) and (b). The prior is a σ Be–N bond, which is slightly polarised towards the nitrogen atom, which reflects the electronegativity difference between the bonding partners. The latter is a π interaction, which is mostly localised on the nitrogen atom and can be interpreted as donation of the lone pair at nitrogen into the empty p orbital of beryllium. This is supported by the fact that only p-orbitals of beryllium and nitrogen are involved, while in the σ Be–N bond also considerable s-orbital contribution is present (see ESI Table S3† for further details). This π interaction is also the cause for the planarisation at the terminal nitrogen atoms. The interaction of the bridging nitrogen atoms with the beryllium atoms consists of four very similar 2-electron–3-centre σ bonds, which contain significant s and p orbital contributions from all bonding partners (Fig. 4c and ESI Table S4†). These bonds are polarised towards the nitrogen atom, but less than in the terminal σ Be–N bonds. Also there is significantly stronger polarisation towards the central beryllium atom. Additionally there are two π type 2-electron–3-centre bonds, which are highly polarised towards the nitrogen atom as well as two further interactions of the terminal beryllium atoms with one of the bridging nitrogen atoms, each (Fig. 4d and ESI Table S5†). These Be–N interactions are also highly polarised towards nitrogen and are mainly composed of one p atomic orbital of nitrogen. All N–C bonds in **1** are σ bonds and no indication for π delocalisation over the N–C bond into the aryl systems was found (ESI Fig. S38 and Table S6†). While there is no N–C bond polarisation in the terminal amido ligands, in the bridging ligands these bonds are slightly polarised towards nitrogen. In non-coordinated H_2NMes, the N–C bond is slightly more polarised towards the nitrogen atom, and also shows no sign of π delocalisation (ESI Fig. S39, S40 and Table S7†).

One- and two-dimensional ^1H and ^{13}C NMR experiments show that the solid state structure of **1** is also retained in solution. However, two isomers with a ratio of roughly two-to-one are present in solution. According to phase selective NOESY experiments, **1** is dynamic in solution and not only the expected exchange between inequivalent methyl and aryl proton signals is observed, but also exchange between the mesityl and NH groups of the two isomers. Interestingly the latter exchange is more pronounced than exchange between terminal and bridging amide units. The exchange between terminal and bridging units is comparable to $[BePh_2]_3$ [40] and is in contrast to $[Be(O^tBu)_2]_3$, which exhibits no dynamic behaviour in solution.[65] Due to the dynamic behaviour in solution, no ^9Be NMR signals of the tri-coordinated beryllium nuclei could be observed. These signals are expected to be broad due to the low symmetry around the quadrupolar ^9Be nuclei[70,71] and the dynamic behaviour of **1** broadens these signals to an extent that they are not observable with the applied NMR experiment. The ^9Be NMR signals of the central beryllium atoms of the major and minor isomer are observed at 6.6 ppm ($\omega_{1/2}$ = 7.0 Hz) and 5.3 ppm ($\omega_{1/2}$ = 5.6 Hz), respectively. These chemical shifts are in line with other beryllium amido complexes[72] and the line widths are indicative for tetra-coordinated beryllium nuclei with high symmetry.[71]

To evaluate the stability of **1** towards coordinating ligands, it was dissolved in pyridine (py). This led to immediate formation of $[(py)_2Be(HNMes)_2]$ (**2**, Fig. 2) as evident from the ^1H and ^{13}C NMR spectra. This reaction is in line with similar reactions performed with heteroleptic beryllium amides of the constitution $[(R_2N)BeR']_n$ [73] as well as the formation of $[(py)_2BePh_2]$ from $[BePh_2]_3$ in pyridine.[74] The ^9Be NMR signals of **2** are found at 8.1 ($\omega_{1/2}$ = 288.0 Hz) and 6.8 ($\omega_{1/2}$ = 131.7 Hz) in C_6D_6 and pyridine-d_5, respectively. These chemical shifts are typical for tetra-coordinated pyridine adducts of beryllium.[74] However, the broad linewidths might indicate partial dissociation of one pyridine ligand in solution. Slow solvent evaporation from a benzene solution of **2** resulted in the formation of crystals suitable for single crystal X-ray diffraction analysis. **2** crystallises in the monoclinic space group *I*2/*a* (15) with four formula units per unit cell. The complex comprises a beryllium atom with a pseudo-tetrahedral coordination sphere, coordinated by two amido and two pyridine ligands as depicted in Fig. 5.

The Be–N bonds to the amido ligands in **2** are, with 1.6557 (14) Å slightly longer than those to the non-bridging amides in **1**. This would be expected due to the higher coordination number at the beryllium atom in **2**. The Be–N bonds to the pyridine ligands are significantly longer at 1.8312(19) Å, which is in accordance with the dative nature of this bond. The respective Be–N bonds in $[(py)_2BePh_2]$ (1.800(3) Å)[74] are slightly shorter, which might indicate that amides are better donor ligands for beryllium than aryls. The N–Be–N angles in **2**

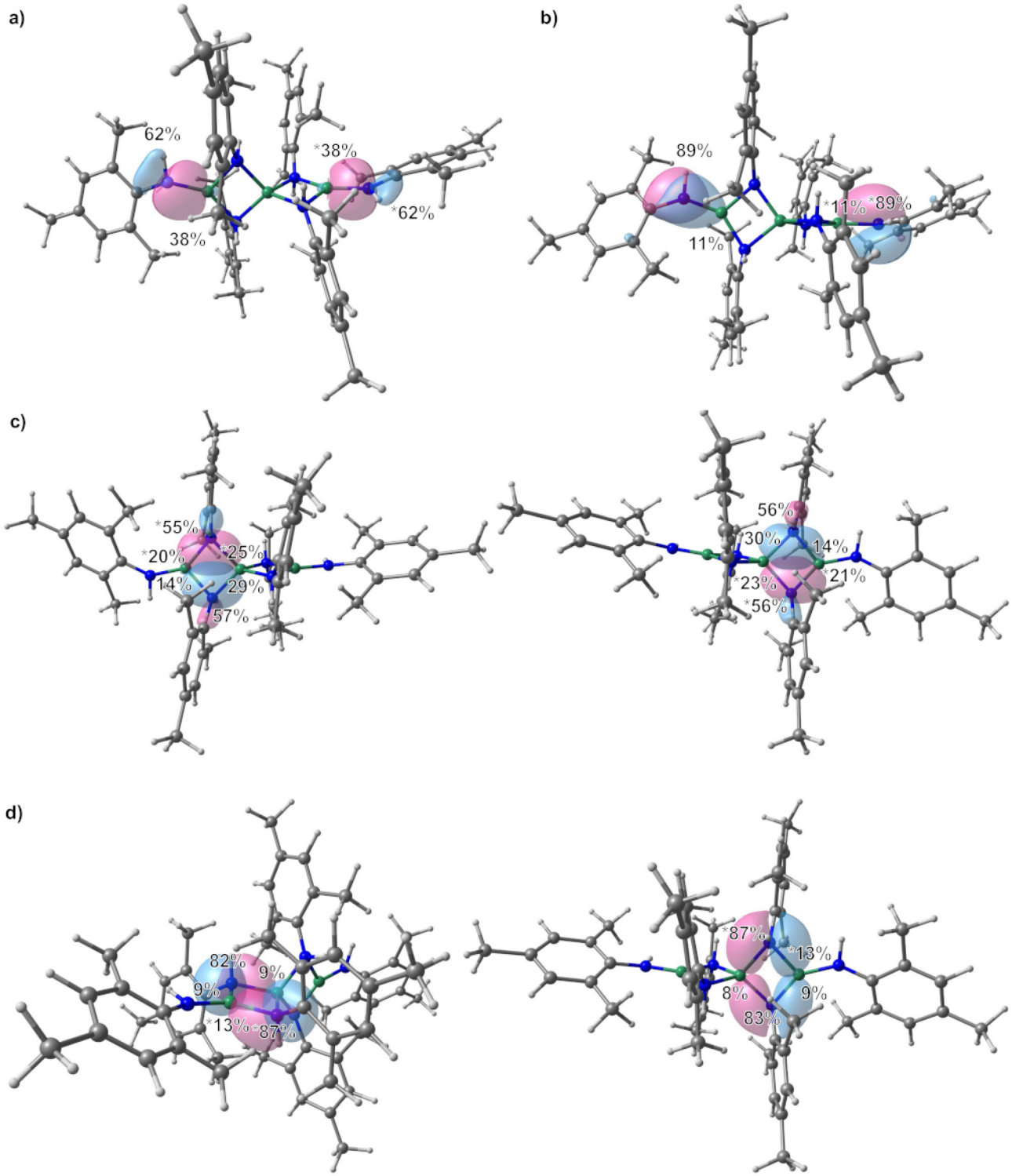

Fig. 4 Localized molecular orbitals (LMOs) showing the Be–N bonds of **1**, with a contour value for the LMO isosurface of 0.05 a.u. Percentages indicate the contribution of each atom to the LMO. The larger the percentage, the more polarized the bond. If the summation does not add up to 100%, then other atoms contribute less than 2% to the LMO. To distinguish between the two LMOs per picture one contribution is marked with an asterisks, each. Be: green, N: blue, C: grey, H: white; red: positive phase, blue: negative phase.

deviate strongly from the ideal tetrahedron angle. This is caused by the significantly higher steric demand of the amido in comparison to the pyridine ligands.

In **2**, the IAO atomic charge at beryllium is with 1.49 comparable to those found in **1**, while the charge at the amido nitrogen is slightly less negative (−0.93, ESI Fig. S29†). The

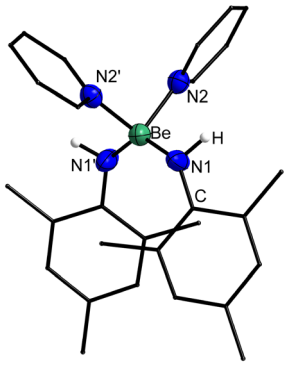

Fig. 5 Solid state structure of **2**. Ellipsoids are depicted at 70% probability at 100 K, while hydrogen atoms are shown isotropic with arbitrary radii. Carbon bound hydrogen atoms are omitted and carbon atoms shown as wire-frame for clarity. Selected bond lengths (Å) and angles (°): Be–N1 1.6557(14), Be–N2 1.8312(19); N1–Be–N1′ 131.5(1), N2–Be–N2′ 98.4(1), N1–Be–N2 103.41(6)–107.75(6).

IAO atomic charge at the pyridine nitrogen atom is, with −0.35 significantly lower than in free pyridine (−0.28, ESI Fig. S30†). LMO analysis of **2** reveals two interactions between the amido ligand and the beryllium atom. One is a σ Be–N bond, which is highly polarised towards the nitrogen atom (Fig. 6a and ESI Table S8†) and is composed of s and p atomic orbital contributions of both atoms. The second interaction (Fig. 6b) is even more polarised towards nitrogen, and is almost exclusively composed of p atomic orbitals, meaning it can be interpreted as a slight donation of the lone pair at nitrogen towards beryllium. Again, no π delocalisation into the aryl system of the amido ligand was observed, and the N–C σ bond polarisation is comparable to the bridging amido ligands in **1**. The Be–N bond to the pyridine ligands is of σ symmetry (Fig. 6c) and the bond polarisation is in between those found for the two Be–N interactions with the amido ligand in **2**.

In analogy to the reactivity of H_2NMes, treatment of a benzene solution of $BeEt_2$ with 2,6-diisopropylaniline (H_2NDipp) led to immediate gas evolution. But again, full conversion was only achieved through heating to 70 °C for 20 h. Even though this reaction is quantitative according to NMR spectroscopy, homoleptic beryllium amide $[Be(HNDipp)_2]_2$ (**3**) could only be isolated in a moderate yield of 55% (Fig. 2). **3** is well soluble in benzene and crystals suitable for single crystal X-ray diffraction analysis could be obtained by slow solvent evaporation. The complex crystallises in the monoclinic space group $P2_1/c$ (14) with two formula units per unit cell. Dinuclear **3** comprises two beryllium atoms which are μ_2-bridged by two amido nitrogen atoms (Fig. 7). Each beryllium atom is additionally coordinated by a terminal amido ligand. The Be⋯Be, Be–N2 and Be–N1 distances are, with 2.269(2), 1.6879(14)–1.7350(14) and 1.5567(14) Å, respectively, comparable to **1**. The two terminal amido ligands are tilted by approximately 20° out of the plane of the four-membered Be–N–heterocycle, which is presumably due to steric repulsion. While the bridging nitrogen atoms of **3** are pseudo-tetrahedrally coordinated, the terminal nitrogen atoms exhibit trigonal planar coordination spheres. These coordination geometries are in analogy to **1**.

The solid state structure of **3** is retained in solution, as evident from two signal sets of 2,6-diisopropylphenylamido ligands in a one-to-one ratio in the ^{1}H and ^{13}C NMR spectra. No indications of dynamic behaviour were observed in these NMR experiments at ambient temperature. The ^{9}Be NMR chemical shift and linewidths of **3** are, with δ = 12.2 ppm and $\omega_{1/2}$ = 281.6 Hz, in the typical range of tri-coordinated beryllium amide complexes.[71,72]

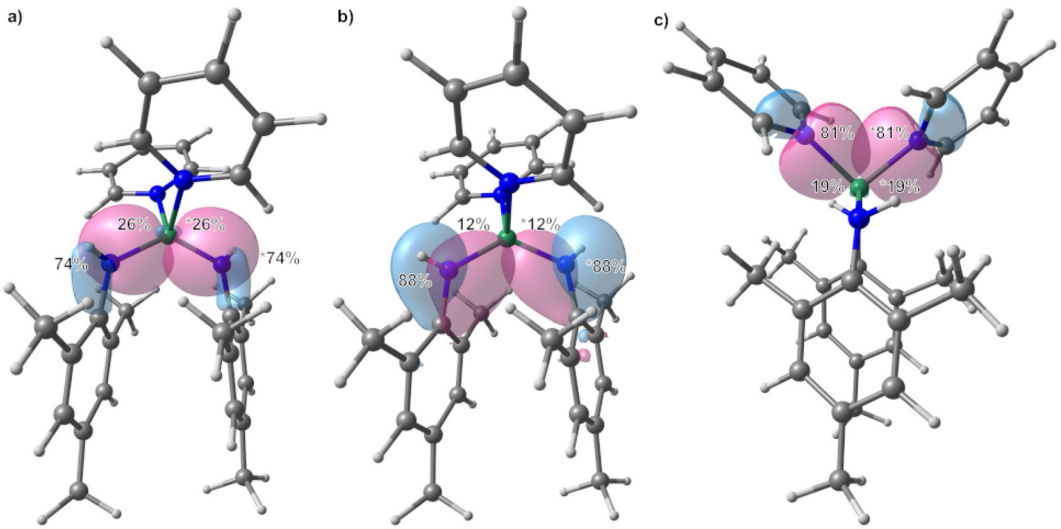

Fig. 6 Localized molecular orbitals (LMOs) showing the Be–N bonds of **2**, with a contour value for the LMO isosurface of 0.05 a.u. Percentages indicate the contribution of each atom to the LMO. The larger the percentage, the more polarized the bond. If the summation does not add up to 100%, then other atoms contribute less than 2% to the LMO. To distinguish between the two LMOs per picture one contribution is marked with an asterisks, each. Be: green, N: blue, C: grey, H: white; red: positive phase, blue: negative phase.

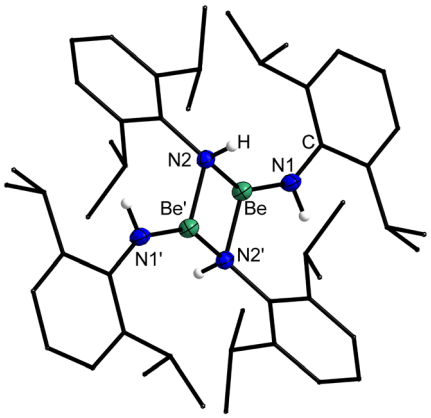

Fig. 7 Solid state structure of **3**. Ellipsoids are depicted at 70% probability at 100 K, while hydrogen atoms are shown isotropic with arbitrary radii. Carbon bound hydrogen atoms are omitted and carbon atoms shown as wire-frame for clarity. Selected bond lengths (Å) and angles (°): Be···Be 2.269(2), Be–N2/2′ 1.6879(14)–1.7350(14), Be–N1 1.5567(14); Be–N2–Be 83.05(7), N2–Be–N2′ 96.95(7), N2–Be–N1/1′ 117.26(8) & 143.43(9), N1–Be–Be′ 161.36(11), N1–Be–N2–Be 159.9(2) & 166.66(9), N1–Be–Be′–N1′ 180.0(2).

In **3** the IAO atomic charges at the beryllium atoms are with 1.51 comparable to **1**, which also applies for the charge at the terminal nitrogen atoms of −0.95 (ESI Fig. S31†). The charge at the bridging nitrogen atoms of **3** is with −1.01 comparable to those found in **1**. Just as in **1**, the deprotonated ligands in **3** show increased negative charge at the nitrogen atoms in comparison to free H_2NDipp (ESI Fig. S32†). The IAO atomic charge at the nitrogen bound carbon atom of the terminal amido ligand is not significantly different to free H_2NDipp, while this charge is slightly reduced in the bridging amido ligand. Analogous to **1**, LMO analysis of **3** gives a σ Be–N bond to the terminal amido ligands (Fig. 8a), which is composed of s and p orbitals of both atoms (ESI Table S11†) and is even less polarized than in **1**. While a π interaction between nitrogen and beryllium was found in **1**, a 2-electron–3-centre π bond is found in **3** (Fig. 8b), which is mostly localised on the nitrogen atom and can be interpreted as donation of the lone pair at nitrogen into the empty p orbital of beryllium as well as into the aromatic π system. The bridging nitrogen atoms of **3** form two 2-electron–3-centre σ bonds with the beryllium atoms, which are polarised towards nitrogen, as well as to one of the beryllium atoms each (Fig. 8c). Two further interactions of one of the beryllium atoms with one of the bridging nitrogen atoms, each are found (Fig. 8d and ESI Table S12†), which are highly polarised towards nitrogen and are mainly composed of one p atomic orbital of nitrogen. These bridging interactions are comparable to the analogous bonds in **1**. Interestingly, two agostic interactions between beryllium and the CH groups of two iso-propyl moieties were calculated (Fig. 8e and ESI Table S13†). The N–C bonds in **3** are σ bonds and, besides the above mentioned 2-electron–3-centre π bond, no indication for further π delocalisation over the N–C bonds into the aryl systems was found (ESI Fig. S42 and Table S14†). The N–C bond polarisation in **3** and comparison of **3** to non coordinated H_2NDipp (ESI Fig. S43, S44 and Table S15†) gives analogous results to **1**.

To evaluate the influence of the nature of the amide ligands more finely, a comparison between two different amido ligands bound in the same complex was necessary. Therefore, a benzene solution of $[(NPh_2)BePh]_2$ [59,65] was reacted with H_2NMes. After one hour of sonication, this gave heteroleptic $[Be(NPh_2)(\mu_2\text{-}HNDipp)]_2$ (**4**, Fig. 9) in quantitative yield, according to NMR spectroscopy. The constitution of **4** in solution could be derived from ^{1}H and ^{13}C NMR spectra, which show one signal set for a diphenylamido and a 2,6-diisopropylphenylamido ligand, each, and no sign for dynamic behaviour at ambient temperature. The ^{9}Be NMR shift of 12.4 ppm and line width of $\omega_{1/2}$ = 275.5 Hz are indicative for tri-coordinated beryllium nuclei.[71,72]

4 dissolves readily in benzene, and crystals suitable for single crystal X-ray diffraction could be grown by slow evaporation of this solvent. The compound crystallises in the monoclinic space group $P2_1/c$ (14) with two formula units per unit cell. Heteroleptic dinuclear **4** is composed of two beryllium atoms, which are μ_2-bridged by the nitrogen atoms of two 2,6-diisopropylphenylamido ligands as depicted in Fig. 10. Each beryllium atom is additionally coordinated by one diphenylamido ligand. The Be···Be distance is with 2.263(4) Å identical to the one in **3** but longer than in $[(NPh_2)BePh]_2$.[65] The Be–N2 and Be–N1 distances are with 1.705(2) & 1.706(2) and 1.574(2) Å, respectively, comparable to **1**, **3** and $[(NPh_2)BePh]_2$.[65] Unlike in **3**, the two terminal amido ligands in **4** are only slightly tilted (aprox. 7°) out of the plane of the four-membered Be–N–heterocycle. The terminal nitrogen atoms of **4** exhibit trigonal planar coordination spheres, while the bridging nitrogen atoms are pseudo-tetrahedrally coordinated, like in **1** and **3**.

The IAO atomic charges at the beryllium atoms of **4** are with 1.50–1.51 identical to those found in **3** (ESI Fig. S33†). This also applies for the charges at the bridging nitrogen atoms of the 2,6-diisopropylphenylamido ligands, with −1.02–1.03. The charges at the nitrogen atoms of the diphenylamido ligands are with −0.75–0.79 the least negative charges found. Again, these charges are significantly more negative than in free H_2NDipp and $HNPh_2$ (ESI Fig. S34†) and the charges at the nitrogen bound carbon atoms do not change considerably. The charge at the nitrogen atoms of the diphenylamido ligands in $[(NPh_2)BePh]_2$ is −0.86 (ESI Fig. S35†) and, therefore, slightly lower than in **4**. This is presumably caused by the bridging coordination mode in $[(NPh_2)BePh]_2$. The charge at the beryllium atom in $[(NPh_2)BePh]_2$ is with 1.45 slightly lower than in the other complexes, which might indicate better donor properties of the phenylido ligand compared to the amido ligands. The LMO analysis of **4** reveals essentially the same bonding modes as in **3**. However, the 2-electron–3-centre σ bonds from the bridging nitrogen to the two beryllium atoms are less polarised between the two beryllium atoms and are more comparable to the bridging interactions in **1**. This is also the case for the other two interactions which are mainly composed of p orbitals at the bridging nitrogen

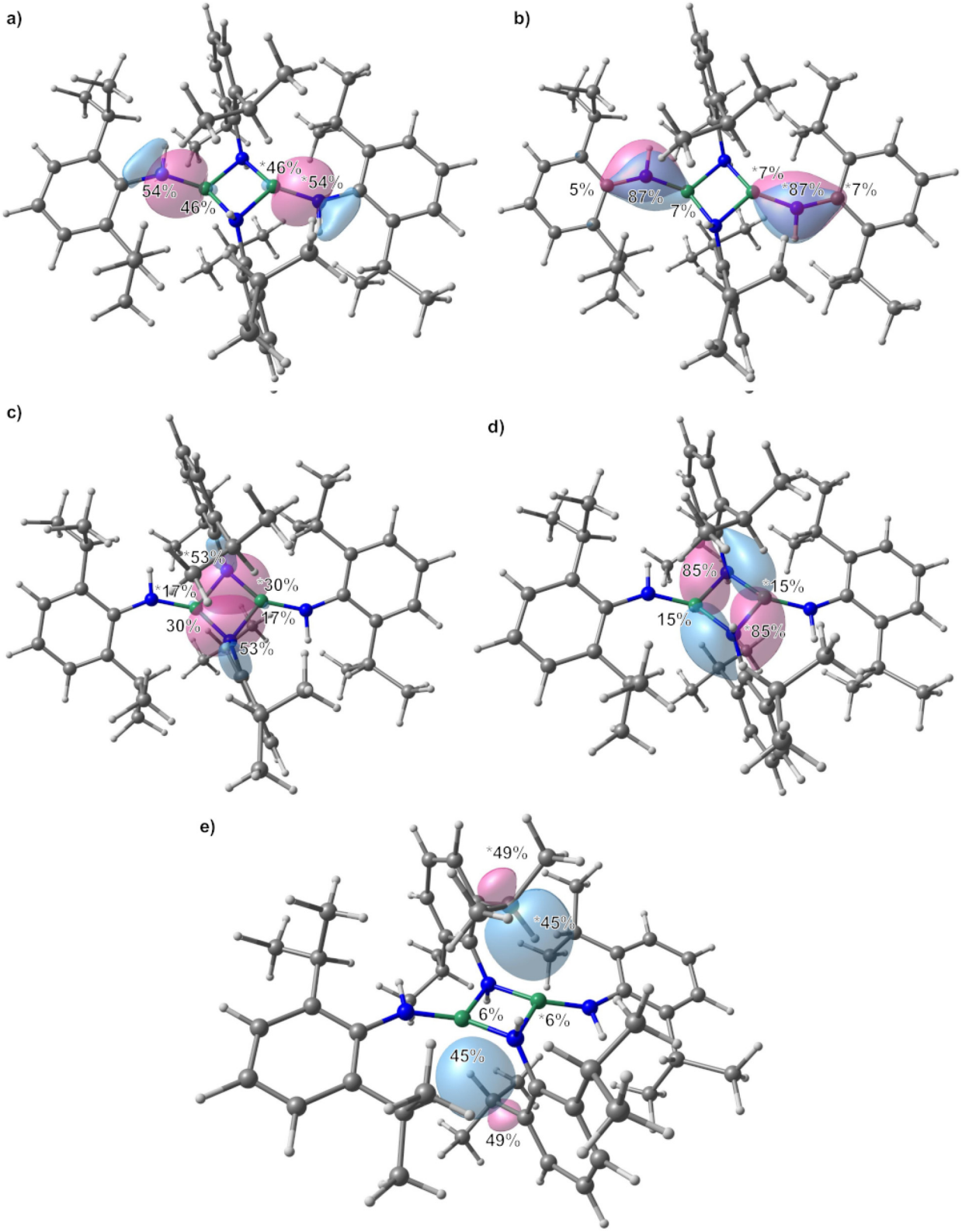

Fig. 8 Localized molecular orbitals (LMOs) showing the Be–N bonds of **3**, with a contour value for the LMO isosurface of 0.05 a.u. Percentages indicate the contribution of each atom to the LMO. The larger the percentage, the more polarized the bond. If the summation does not add up to 100%, then other atoms contribute less than 2% to the LMO. To distinguish between the two LMOs per picture one contribution is marked with an asterisks, each. Be: green, N: blue, C: grey, H: white; red: positive phase, blue: negative phase.

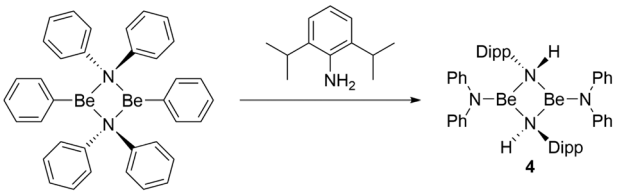

Fig. 9 Reaction of $[(NPh_2)BePh]_2$ [59,65] with 2,6-diisopropylaniline (H_2NDipp).

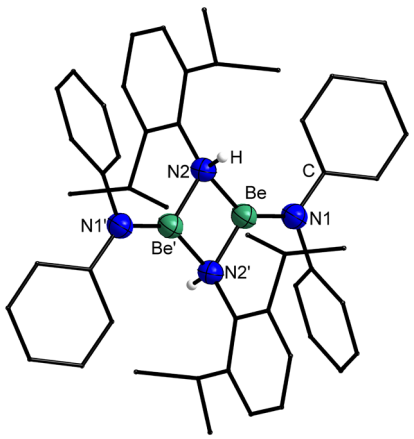

Fig. 10 Solid state structure of **4**. Ellipsoids are depicted at 70% probability at 100 K, while hydrogen atoms are shown isotropic with arbitrary radii. Carbon bound hydrogen atoms are omitted and carbon atoms shown as wire-frame for clarity. Selected bond lengths (Å) and angles (°): Be···Be 2.263(4), Be–N2/2′ 1.705(2) & 1.706(2), Be–N1 1.574(2); Be–N2–Be′ 83.1(1), N2–Be–N2′ 96.9(1), N2–Be–N1 125.2(1) & 137.9(1), N1–Be–Be′ 173.37(17), N1–Be–N2–Be′ 177.4(2) & 177.8(2), N1–Be–Be′–N1′ 180.0(10).

atoms (ESI Fig. S45 and Table S16†). While the Be–N σ bond to the terminal diphenylamido ligands is essentially identical to the respective one in **3**, there is only one 2-electron–3-centre π interaction on one side and some donation of the lone pair at the nitrogen atoms into the p orbitals of the beryllium atoms on the other side of the molecule (ESI Fig. S46 and Table S17†). The C–N bonds are exclusively of σ symmetry in **4** and free $HNPh_2$ with no indication for π delocalisation into the aromatic ring (ESI Fig. S47–S49 and Tables S18–S19†). In $[(NPh_2)BePh]_2$ the Be–C bonds are exclusively of σ symmetry, with almost no bond polarisation (ESI Fig. S50 and Table S20†). The bridging interaction between the nitrogen atoms and the beryllium atoms consists of two 2-electron–3-centre σ bonds, which are basically identical to those in **4** (ESI Fig. S51 and Table S21†). However, there are two additional 2-electron–3-centre interactions, which are composed mainly of one of the p orbitals at the nitrogen atoms each (ESI Fig. S51 and Table S21†). This might indicate that the poorer donating properties of the phenylido ligands are compensated through multi-centre bonding between beryllium and nitrogen. The N–C bonds in **4** and $[(NPh_2)BePh]_2$ are very similar (ESI Fig. S52 and Table S22†).

Since some electron density is delocalised over the C–N–Be bonds in **3** and **4**, we wanted to study the influence of more efficient delocalisation onto the structure of the corresponding beryllium complex. We therefore, reacted an etheral solution of $Be(^iBu)_2$ with diphenylmethaneimine ($HNCPh_2$). This resulted in immediate gas evolution. However, complete conversion, according to NMR spectroscopy, was only achieved through heating to 65 °C over 20 h. This gave brightly yellow $[Be(NCPh_2)_2]_3$ (**5**) in an isolated yield of 53% (Fig. 11). **5** is reasonably soluble in aromatic solvents and exhibits two singlets with a one-to-two ratio at 6.0 ppm ($\omega_{1/2}$ = 21.5 Hz) and 6.7 ppm ($\omega_{1/2}$ = 17.5 Hz) in the ^{9}Be NMR spectrum. This is indicative for a trinuclear linear compound, which is also supported by the presence of two signal sets of diphenylmethaneimido ligands with one-to-two ratio in the ^{1}H and ^{13}C NMR spectra.

Crystals of **5** suitable for single crystal X-ray diffraction analysis could be grown by slow solvent evaporation from a saturated Et_2O solution. Trinuclear **5** crystallises in the triclinic space group $P\bar{1}$ (2) with two formula units per unit cell and comprises a central tetra-coordinated beryllium atom, which is μ_2-bridged by four imide nitrogen atoms to two terminal beryllium atoms. These terminal beryllium atoms are further coordinated to one nitrogen atom of a non-bridging imido ligand each and exhibit a trigonal planar coordination sphere (Fig. 12). This structure is closely related to **1**, however, **5** is significantly more linear with a Be–Be–Be angle of 179.1(1)°. While in **1** the angle between the trigonal planes of the terminal beryllium atoms is almost 90°, in **5** this angle is with 74.6(1)° significantly smaller. The Be···Be separations in **5** are with 2.330(3) and 2.339(3) Å comparable to those in **1** and by tendency longer than in the dinuclear compounds. The Be–N bonds to the terminal imido nitrogen atoms are with 1.502(3) and 1.507(3) Å shorter than those to the bridging nitrogen atoms. The Be–N distances from the central beryllium atom to the bridging nitrogen atoms are with 1.718(3)–1.728(3) Å considerably longer than those to the terminal beryllium atoms (1.668(3)–1.674(3) Å). All Be–N bonds in **5** are by tendency shorter than in complexes **1**, **2**, **3**, **4** and $[(NPh_2)BePh]_2$. In the terminal imido ligands the nitrogen atoms are almost linearly coordinated, with Be–N–C angles of 175.8(2)° and 176.7(2)° and the CPh_2 plane is standing almost perpendicular to the BeN_3 plane. In contrast to this, the CPh_2 plane of the bridging imido ligands is parallel to the NBe_2 plane.

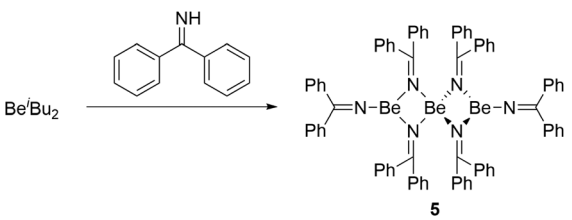

Fig. 11 Reaction of diisobutyl beryllium with diphenylmethanimine ($HNCPh_2$).

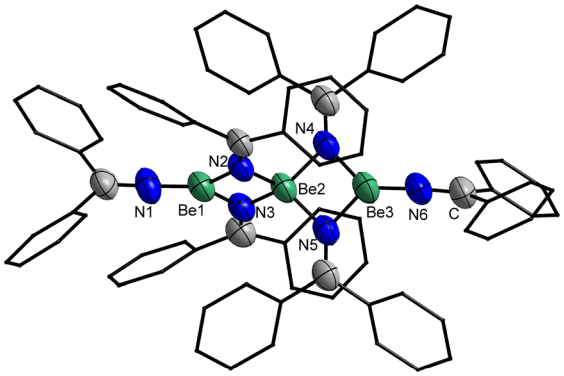

Fig. 12 Solid state structure of **5**. Ellipsoids are depicted at 70% probability at 100 K. Hydrogen atoms are omitted and phenyl carbon atoms shown as wire-frame for clarity. Selected bond lengths (Å) and angles (°): Be···Be 2.330(3) & 2.339(3), Be1/3–N_μ 1.668(3)–1.674(3), Be2–N_μ 1.718(3)–1.728(3), Be1/3–N1/6 1.502(3) & 1.507(3), N_μ–C 1.270(2)–1.280(2), N1/6–C 1.253(2), 1.264(2); Be1/3–N_μ–Be2 86.7(1)–87.3(1), N_μ–Be2–N_μ 91.2(1)–110.7(1), N_μ–Be1/3–N_μ 84.7(1)–95.2(1), N1/6–Be1/3–N_μ 130.5(2)–134.3(2), N1/6–Be1/3–Be2 176.7(2) & 179.6(1), Be1–Be2–Be3 179.1(1), N1/6–Be1/3–N_μ–Be2 176.2(3)–179.9(3); angle between Be1/3N_3 planes: 74.6(1)°.

The IAO atomic charges at the beryllium atoms of **5** are, with 1.49–1.51, comparable to those in all other investigated compounds (ESI Fig. S36†). The charges at the bridging nitrogen atoms are with −0.96 significantly more negative than at the terminal nitrogen atoms (−0.90), which is in line with the complexes described above. Also, the deprotonated ligands show significantly more negative partial charges at the nitrogen atoms in comparison to free $HNCPh_2$ (ESI Fig. S37†). The IAO atomic charges at the nitrogen bound carbon atom of the terminal imido ligands and free $HNCPh_2$ are almost identical, while the respective charges in the bridging imido ligands are slightly higher. For the interaction of the bridging nitrogen atoms with the beryllium atoms, the LMO analysis of **5** reveals four identical 2-electron–3-centre σ bonds, which compare well to those found in **1** (ESI Fig. S53 and Table S23†). Additionally, π type 2-electron–4-centre bonds were found, which are polarised towards the nitrogen atom, but do have comparable contributions of the nitrogen bound carbon atom as well as of the beryllium atoms (ESI Fig. S54 and Table S23†). The terminal Be–N bonds consist of one σ bond each, which exhibits a 60% polarisation towards nitrogen and is, therefore, comparable to those in the other compounds (ESI Fig. S55 and Table S24†). Additionally, however, there is a 2-electron–3-centre π bond, which is in comparison to the other complexes significantly more delocalised (N 76%, Be 10%, C 14%). All N=C bonds consist of very slightly polarised σ bonds and π bonds that are polarised slightly more towards nitrogen (ESI Fig. S56–S58 and Table S25†). These two bonds are only slightly altered in **5** in comparison to free $HNCPh_2$ (ESI Fig. S59, S60 and Table S26†). Interestingly, the lone pair at nitrogen in free $HNCPh_2$ is slightly donating into the p orbital of the adjacent carbon atom. Such an interaction was not observed for the other ligands.

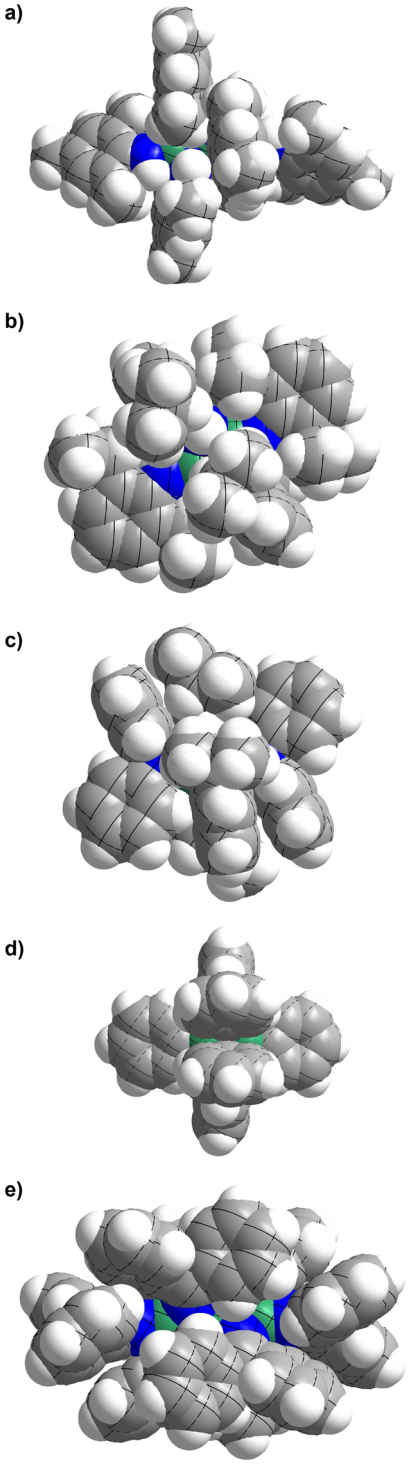

Fig. 13 Space filling models of (a) $[Be(HNMes)_2]_3$ (**1**), (b) $[Be(HNDipp)_2]_2$ (**3**), (c) $[Be(NPh_2)(\mu_2\text{-}HNDipp)]_2$ (**4**), (d) $[(NPh_2)BePh]_2$[65] and (e) $[Be(NCPh_2)_2]_3$ (**5**). Be: green, N: blue, C: grey, H: white.

3 Conclusions

In summary we have prepared a set of closely related beryllium amide and imide complexes: $[Be(HNMes)_2]_3$ (**1**), $[(py)_2Be$

$(HNMes)_2]$ (**2**), $[Be(HNDipp)_2]_2$ (**3**), $[Be(NPh_2)(\mu_2\text{-}HNDipp)]_2$ (**4**) and $[Be(NCPh_2)_2]_3$ (**5**). These compounds are all well soluble in aromatic solvents, which is in contrast to many related organo beryllium complexes. With exception of **1** and **2** no evidence for dynamic behaviour in solution was observed. IAO atomic charge analysis revealed no significant differences in the charge distributions of the multinuclear compounds or the mononuclear pyridine adduct **2**. LMO analysis showed that the Be–N interactions to the terminal amido ligands mainly consist of covalent σ Be–N bonds, while the μ_2-N bridging interactions are 2-electron–3-centre σ bonds. The electron deficiency at the beryllium atoms is partially compensated through additional donation from the lone pairs at the nitrogen atoms to the beryllium atoms. This results in a partial double bond character of the terminal Be–N bonds and is the reason for the planarisation of the terminal nitrogen atoms. In case of the bridging nitrogen atoms, the lone pair at nitrogen stays mainly located at the nitrogen atom and only slightly donates to one or two beryllium atoms. This multi-centre bonding is favoured if the 2-electron–3-centre σ bond is equally distributed over the participating beryllium atoms. π delocalisation over the terminal Be–N–C and bridging Be_2–N–C bonds is possible, if the molecular geometry allows for it and can be enforced through introduction of imido ligands, which contain N=C double bonds. However, this π delocalisation has no significant effect on the partial charge distribution at the beryllium and nitrogen atoms. In conclusion, alteration of the electronic properties of the N-donor ligands has little influence on the bonding situation. It is more likely that the steric demand of the ligands dictates the structure of the beryllium compounds, which is illustrated in the space filling models depicted in Fig. 13.

4 Experimental procedures

Caution! Beryllium and its compounds are categorized as human carcinogens and work with these substances is associated with severe health hazards.[75] As the biochemical mechanisms that cause beryllium associated diseases are still unknown,[76–78] special (safety) precautions are strongly advised.[75]

4.1 General experimental techniques

All manipulations were performed either under solvent vapor pressure or dry argon using a glovebox and Schlenk techniques. C_6D_6 was dried over NaK alloy, while for C_6H_6, *n*-pentane and Et_2O sodium was used. Pyridine (py) and pyridine-d_5 (py-d_5) were dried over CaH_2. All solvents were subsequently vacuum distilled before storage in an argon filled glovebox. $BeEt_2$,[26,27,79] $Be(^iBu)_2$ [26,27,79] and $[(NPh_2)BePh]_2$ [65] were prepared according to the literature. 2,4,6-Trimethylaniline (H_2NMes), 2,6-diisopropylaniline (H_2NDipp) and diphenylmethanimine ($HNCPh_2$) were purchased from commercial vendors and vacuum distilled prior to use. All reactions were carried out in J. Young NMR tubes or PTFE sealed Schlenk tubes. All glassware was silylated according to the procedure in the ref. 80. Due to the expected extreme toxicity of the obtained compounds, no elemental analysis or mass spectrometry could be performed.

NMR spectroscopy. ^1H, ^9Be and ^{13}C NMR spectra were recorded on Bruker Avance Neo 300 and Avance III 500 NMR spectrometers. The latter was equipped with a Prodigy CryoProbe. ^1H NMR (300/500 MHz) and ^{13}C NMR (76/126 MHz) chemical shifts are given relative to the solvent signal for C_6D_6 (7.26 and 77.2 ppm), while ^9Be (42 MHz) used 0.43 [M] $BeSO_4$ in D_2O as an external standard. NMR spectra were processed with the MESTRENOVA software package.[81]

IR spectroscopy. IR spectra were recorded on a Bruker alpha FTIR spectrometer equipped with a diamond ATR unit in an argon filled glovebox. Processing of the spectra was performed with the OPUS software package[82] and MESTRENOVA.[81]

Single crystal X-ray diffraction. Single crystals were selected under a pre-dried argon stream in perfluorinated polyether (Fomblin YR 1800, Solvay Solexis) and mounted using the MiTeGen MicroLoop system at ambient temperature. X-ray diffraction data was collected using the monochromated Cu-K_α (λ = 1.54186 Å) radiation of a Stoe StadiVari diffractometer equipped with a Xenocs Microfocus Source and a Dectris Pilatus 300 K detector or a Bruker D8 Venture diffractometer equipped with a PHOTON III C14 detector. Evaluation, integration and reduction of the diffraction data was carried out using the X-AREA[83] or the APEX5[84] software suites. Multi-scan absorption correction was applied with the LANA module of the X-AREA[83] software suite or with SADABS.[85] The structures were solved with dual-space methods (SHELXT-2018/2) and refined against F^2 (SHELXL-2018/3) using the SHELXLE software package.[86–88] Non-hydrogen atoms were refined anisotropically. Hydrogen atoms were refined using the "riding model" approach with isotropic displacement parameters 1.5 times of that of the preceding carbon atom. For the crystal data and details of the structure determination see Tables S1 and S2.†

Computational details. All Density Functional Theory (DFT) calculations were conducted with the program suite TURBOMOLE 7.7[89,90] using the PBE0 hybrid density functional method (DFT-PBE0)[91,92] and the Karlsruhe triple-ζ valence basis set with one sets of polarizations functions (def2-TZVP).[93] Grimme's third generation dispersion correction with the Becke–Johnson damping scheme was employed.[94–96] Multipole-accelerated resolution-of-the-identity approximation (MA-RIJ) was used to speed up the DFT calculations[97–99] and standard m4 integration grids for the numerical integration of the exchange–correlation part were used. All structures were optimized within their respective point group symmetry in the gas phase. The optimized structures were confirmed to be true local minima with numerical harmonic frequency calculations, as implemented in TURBOMOLE. The Cartesian coordinates of the optimized and point group symmetry of the molecular structures are included in the ESI.† LMOs using the IBO localization method, IAO atomic charge analysis and Natural Population Analysis (NPA) were calculation with the PROPER program implemented in TURBOMOLE.[68,100] The results of

the default IAO basis did not reproduce the results in the program IBOVIEWER. The IAO basis was changed in TURBOMOLE to the values shown in ESI Table S37.† The default Mulliken contribution threshold of 0.1 was retained, and negative and minor d and f orbital Mulliken contributions were neglected in the analysis. LMOs were plotted with the program CHEMCRAFT 1.8.[101]

4.2 Synthesis and characterization

[Be(HNMes)$_2$]$_3$ (1). $BeEt_2$ (67.1 mg, 1.00 mmol, 1 eq.) was dissolved in 5 ml benzene and H_2NMes (270.4 mg, 2.00 mmol, 2 eq.) was added. Immediately gas evolution was observed and the reaction mixture was subsequently heated to 70 °C for 20 h. The solvent was removed from the pale yellow solution *in vacuo*. The obtained pale yellow solid was washed with 5 ml *n*-pentane to give the title compound as a colourless solid in 64% (176.4 mg) isolated yield. Single crystals were obtained from an oversaturated benzene solution. ^{1}H NMR (500 MHz, C_6D_6) δ = major isomer: 1.82 (s, 6H, CH_3), 2.02 (s, 6H, CH_3), 2.08 (s, 3H, CH_3), 2.16 (s, 6H, CH_3), 2.35 (s, 6H, CH_3), 3.30 (bs, 1H, N*H*), 3.33 (bs, 2H, N*H*), 6.62 (s, 2H, C*H*$_{Ar}$), 6.64–6.67 (m, 2H, C*H*$_{Ar}$), 6.79–6.82 (m, 1H, C*H*$_{Ar}$); minor isomer: 1.89 (s, 6H, CH_3), 1.99 (s, 6H, CH_3), 2.04 (s, 6H, CH_3), 2.08 (s, 3H, CH_3), 2.30 (s, 6H, CH_3), 3.27 (bs, 2H, N*H*), 3.40 (bs, 1H, N*H*), 6.03–6.11 (m, 2H, C*H*$_{Ar}$), 6.64–6.66 (m, 4H, C*H*$_{Ar}$). ^{9}Be NMR (42 MHz, C_6D_6) δ = major isomer: 6.6 (s, $\omega_{1/2}$ = 7.0 Hz); minor isomer: 5.3 (s, $\omega_{1/2}$ = 5.6 Hz); the signals of the tricoordinated Be nuclei were too broad for observation. ^{13}C NMR (126 MHz, C_6D_6) δ = major isomer: 18.5 (s, CH_3), 18.8 (s, CH_3), 20.5 (s, CH_3), 20.7 (s, CH_3), 21.1 (s, CH_3), 124.2 (s, C_{Ar}), 125.1 (s, C_{Ar}), 126.8 (s, C_{Ar}), 128.3 (s, C_{Ar}), 129.3 (s, *C*H$_{Ar}$), 130.4 (s, *C*H$_{Ar}$), 130.9 (s, C_{Ar}), 131.3 (s, *C*H$_{Ar}$), 142.0 (s, *C*N), 145.5 (s, *C*N); minor isomer: 18.9 (s, CH_3), 19.9 (s, CH_3), 20.5 (s, CH_3), 20.6 (s, CH_3), 124.5 (s, C_{Ar}), 125.2 (s, C_{Ar}), 125.5 (s, C_{Ar}), 127.0 (s, C_{Ar}), 129.0 (s, C_{Ar}), 129.4 (s, *C*H$_{Ar}$), 130.2 (s, *C*H$_{Ar}$), 130.5 (s, *C*H$_{Ar}$), 141.3 (s, *C*N), 145.8 (s, *C*N). IR (cm^{-1}): 3341 (vw), 3296 (w), 3008 (w), 2968 (w), 2913 (m), 2853 (m), 2727 (vw), 1613 (w), 1481 (s), 1434 (m), 1401 (w), 1387 (w), 1371 (w), 1348 (w), 1307 (m), 1265 (m), 1232 (w), 1218 (m), 1150 (m), 1048 (m), 1028 (w), 1008 (w), 959 (w), 928 (w), 851 (s), 802 (vs), 746 (w), 732 (s), 693 (m), 642 (w), 612 (m), 598 (w), 575 (m), 559 (s), 516 (m), 496 (w), 463 (m), 445 (w).

[(py)$_2$Be(HNMes)$_2$] (2). $BeEt_2$ (33.5 mg, 0.5 mmol, 1 eq.) was dissolved in 5 ml pyridine and H_2NMes (135.0 mg, 1.00 mmol, 2 eq.) was added. Immediately gas evolution was observed together with a colour change to orange. The reaction mixture was subsequently heated to 70 °C for 20 h. The solvent was removed from the orange solution *in vacuo*. The obtained yellow solid was washed with 5 ml *n*-pentane to give the title compound as a yellow solid in 62% (160.8 mg) isolated yield. Single crystals were obtained from an oversaturated benzene solution. ^{1}H NMR (500 MHz, C_6D_6) δ = 2.17–2.30 (bm, 18H, CH_3), 3.47 (bs, 2H, N*H*), 6.43–6.57 (m, 4H, C*H*$_{py}$), 6.80 (bs, 4H, C*H*$_{Ar}$), 6.82–6.93 (m, 2H), 8.36–8.51 (m, 4H, C*H*$_{py}$). ^{1}H NMR (300 MHz, py-d_5) δ = 2.27 (s, 3H, CH_3), 2.32 (s, 6H, CH_3), 4.55 (s, 1H, N*H*), 6.86 (s, 2H, C*H*$_{Ar}$). ^{9}Be NMR (42 MHz, C_6D_6) δ = 8.1 (bs, $\omega_{1/2}$ = 288.0 Hz). ^{9}Be NMR (42 MHz, py-d_5) δ = 6.8 (bs, $\omega_{1/2}$ = 131.7 Hz). ^{13}C NMR (126 MHz, C_6D_6) δ = 20.0 (bs, CH_3), 20.7 (s, CH_3), 123.9 (s, *C*H$_{py}$), 125.1 (bs, *C*H$_{Ar}$), 129.3 (bs, C_{Ar}) 130.1 (bs, *C*H$_{Ar}$), 136.6 (s, *C*H$_{py}$), 149.6 (s, *C*H$_{py}$); two C_{Ar} signals could not be detected. IR (cm^{-1}): 3443 (w), 3327 (m), 3221 (w), 2998 (w), 2966 (w), 2908 (m), 2853 (m), 1628 (m), 1603 (m), 1560 (m), 1489 (s), 1475 (m), 1442 (s), 1399 (w), 1375 (w), 1303 (s), 1267 (w), 1205 (m), 1152 (m), 1067 (m), 1042 (s), 1010 (s), 959 (w), 938 (m), 916 (s), 885 (w), 855 (s), 830 (m), 740 (s), 704 (vs), 657 (s), 642 (s), 598 (s), 551 (vs), 498 (w), 479 (s), 465 (s), 424 (w).

[Be(HNDipp)$_2$]$_2$ (3). $BeEt_2$ (67.1 mg, 1.00 mmol, 1 eq.) was dissolved in 5 ml benzene and H_2NDipp (354.6 mg, 2.00 mmol, 2 eq.) was added. Immediately gas evolution was observed and the reaction mixture was subsequently heated to 70 °C for 20 h. The solvent was removed from the colourless solution *in vacuo*. The obtained colourless solid was washed with 5 ml *n*-pentane to give the title compound as a colourless solid in 55% (200.0 mg) isolated yield. Single crystals were obtained from an oversaturated benzene solution. ^{1}H NMR (500 MHz, C_6D_6) δ = 0.95 (d, $^3J_{HH}$ = 6.9 Hz, 12H, CH_3), 1.00 (d, $^3J_{HH}$ = 6.8 Hz, 12H, CH_3), 1.28 (d, $^3J_{HH}$ = 6.7 Hz, 24H, CH_3), 2.83 (hept, $^3J_{HH}$ = 6.7 Hz, 4H, $CH(CH_3)_2$), 3.09 (hept, $^3J_{HH}$ = 6.7 Hz, 4H, $CH(CH_3)_2$), 3.65 (s, 2H, N*H*), 3.81 (s, 2H, N*H*), 6.84–6.92 (m, 2H, C*H*$_{Ar}$), 6.93–7.00 (m, 2H, C*H*$_{Ar}$), 7.01–7.07 (m, 8H, C*H*$_{Ar}$). ^{9}Be NMR (42 MHz, C_6D_6) δ = 12.2 (bs, $\omega_{1/2}$ = 281.6 Hz). ^{13}C NMR (126 MHz, C_6D_6) δ = 23.5 (s, CH_3), 23.6 (s, CH_3), 23.8 (s, CH_3), 28.1 (s, $CH(CH_3)_2$), 31.4 (bs, $CH(CH_3)_2$), 118.9 (s, *C*H$_{Ar}$), 123.1 (s, *C*H$_{Ar}$), 123.3 (s, *C*H$_{Ar}$), 124.6 (s, *C*H$_{Ar}$), 136.3 (s, C_{Ar}), 137.4 (s, C_{Ar}), 141.0 (s, *C*N), 144.7 (s, *C*N). IR (cm^{-1}): 3351 (vw), 3302 (vw), 3045 (w), 2959 (m), 2923 (w), 2868 (w), 1615 (w), 1593 (w), 1481 (w), 1460 (m), 1434 (s), 1385 (w), 1354 (m), 1336 (w), 1316 (w), 1297 (w), 1273 (m), 1263 (m), 1228 (m), 1216 (w), 1189 (w), 1150 (w), 1116 (w), 1099 (w), 1052 (s), 1026 (s), 959 (w), 926 (s), 885 (w), 857 (s), 802 (s), 769 (s), 738 (vs), 696 (w), 679 (m), 630 (m), 596 (m), 555 (w), 543 (w), 530 (w), 510 (m), 485 (m), 455 (m), 416 (m).

[Be(NPh$_2$)(μ$_2$-HNDipp)]$_2$ (4). [(NPh$_2$)BePh]$_2$ (12.7 mg, 0.025 mmol, 1 eq.) was dissolved in 0.5 ml C_6D_6 and H_2NDipp (8.86 mg, 0.05 mmol, 2 eq.) was added. The colourless reaction mixture was sonicated for 1 h. Removal of the solvent *in vacuo* gave the title compound as a colourless solid in almost quantitative yield (98%, 17.3 mg). Single crystals were obtained from an oversaturated benzene solution. ^{1}H (300 MHz, C_6D_6) δ = 1.14 (d, $^3J_{HH}$ = 6.7 Hz, 24H, CH_3), 2.75 (hept, $^3J_{HH}$ = 6.6 Hz, 4H, $CH(CH_3)_2$), 3.81 (s, 2H, N*H*), 6.58–6.66 (m, 8H, C*H*$_{Ar}$), 6.65–6.75 (m, 4H, C*H*$_{Ar}$), 6.77–6.91 (m, 8H, C*H*$_{Ar}$), 6.93–7.13 (m, 6H, C*H*$_{Ar}$). ^{9}Be NMR (42 MHz, C_6D_6) δ = 12.4 (bs, $\omega_{1/2}$ = 275.5 Hz). ^{13}C NMR (126 MHz, C_6D_6) δ = 23.2 (s, CH_3), 31.1 (s, $CH(CH_3)_2$), 121.5 (s, *C*H$_{Ar}$), 123.2 (s, *C*H$_{Ar}$), 124.4 (s, *C*H$_{Ar}$), 125.1 (s, *C*H$_{Ar}$), 129.1 (s, *C*H$_{Ar}$), 136.9 (s, C_{Ar}), 142.9 (s, *C*N), 153.0 (s, *C*N). IR (cm^{-1}): 3306 (w), 3051 (w), 3029 (w), 2964 (m), 2931 (w), 2872 (w), 1587 (m), 1485 (s), 1460 (w), 1436 (m), 1387 (w), 1367 (w), 1334 (w), 1265 (s), 1242 (w), 1216 (s), 1179 (m), 1089 (m), 1044 (s), 1026 (w), 997 (m), 930 (w), 914 (w), 891 (s), 879 (s), 857 (w), 816 (m), 787 (m), 773 (w), 753 (vs), 698 (vs),

677 (w), 628 (m), 610 (m), 579 (w), 553 (m), 516 (w), 500 (m), 469 (s), 445 (w), 420 (w).

$[Be(N{=}CPh_2)_2]_3$ (5). $Be(^tBu)_2$ (123.2 mg, 1.00 mmol, 1 eq.) was dissolved in 5 ml Et_2O and $HNCPh_2$ (362.5 mg, 2.00 mmol, 2 eq.) was added. Immediately gas evolution was observed and the red reaction mixture was subsequently heated to 65 °C for 20 h. The solvent was removed *in vacuo*. The obtained yellow solid was washed with 5 ml *n*-pentane to give the title compound as a bright yellow solid in 53% (195.9 mg) isolated yield. Single crystals were obtained from an oversaturated Et_2O solution. ^{1}H NMR (500 MHz, C_6D_6) δ = 6.55–7.28 (m, 52H, CH_{Ar}), 7.56–7.65 (m, 8H, CH_{Ar}). ^{9}Be NMR (42 MHz, C_6D_6) δ = 6.0 (s, $\omega_{1/2}$ = 21.5 Hz, 1Be), 6.7 (s, $\omega_{1/2}$ = 17.5 Hz, 2Be). ^{13}C NMR (126 MHz, C_6D_6) δ = 127.0 (s, CH$_{Ar}$), 127.4 (s, CH$_{Ar}$), 128.6 (s, CH$_{Ar}$), 128.8 (s, CH$_{Ar}$), 129.2 (s, CH$_{Ar}$), 129.3 (s, CH$_{Ar}$), 129.4 (s, CH$_{Ar}$), 129.4 (s, CH$_{Ar}$), 129.7 (s, CH$_{Ar}$), 142.2 (s, C_{Ar}), 143.3 (s, C_{Ar}), 143.8 (s, C_{Ar}), 159.1 (s, C=N), 178.7 (s, C=N). IR (cm^{-1}): 3351 (vw), 3302 (w), 3053 (w), 3025 (w), 2959 (m), 2921 (w), 2864 (w), 1732 (w), 1617 (m), 1595 (w), 1575 (w), 1483 (m), 1460 (n), 1434 (s), 1385 (w), 1356 (m), 1334 (w), 1316 (m), 1297 (w), 1273 (m), 1260 (s), 1230 (m), 1218 (w), 1189 (w), 1154 (w), 1116 (w), 1099 (w), 1052 (s), 1028 (s), 950 (m), 926 (m), 887 (w), 851 (s), 830 (w), 816 (w), 802 (s), 787 (w), 769 (s), 740 (vs), 693 (vs), 679 (m), 645 (w), 628 (s), 598 (w), 587 (w), 557 (w), 543 (s), 510 (m), 485 (w), 455 (w), 434 (w), 422 (m).

Data availability

The data supporting this article have been included as part of the ESI.†

Conflicts of interest

There are no conflicts to declare.

Acknowledgements

M. R. B. thanks Prof. F. Kraus for moral and financial support as well as the provision of laboratory space. The DFG is gratefully acknowledged for financial support (BU2725/8-1).

References

1 C. Jones, *Nat. Rev. Chem.*, 2017, **1**, 0059.
2 J. Hicks, P. Vasko, J. M. Goicoechea and S. Aldridge, *Angew. Chem., Int. Ed.*, 2021, **60**, 1702–1713.
3 C. Czernetzki, T. Kunz, S. Huynh, A. Lamprecht, J. Sprenger, M. Finze, M. Arrowsmith and H. Braunschweig, *Angew. Chem., Int. Ed.*, 2024, **63**, e202401279.
4 I.-A. Bischoff, S. Danés, P. Thoni, B. Morgenstern, D. M. Andrada, C. Müller, J. Lambert, E. C. J. Gießelmann, M. Zimmer and A. Schäfer, *Nat. Chem.*, 2024, **16**, 1093–1100.
5 S. P. Green, C. Jones and A. Stasch, *Science*, 2007, **318**, 1754–1757.
6 J. Hicks, P. Vasko, J. M. Goicoechea and S. Aldridge, *Nature*, 2018, **557**, 92–95.
7 B. Rösch, T. X. Gentner, J. Eyselein, J. Langer, H. Elsen and S. Harder, *Nature*, 2021, **592**, 717–721.
8 B. Rösch, T. X. Gentner, J. Langer, C. Färber, J. Eyselein, L. Zhao, C. Ding, G. Frenking and S. Harder, *Science*, 2021, **371**, 1125–1128.
9 A. Paparo, C. D. Smith and C. Jones, *Angew. Chem., Int. Ed.*, 2019, **58**, 11459–11463.
10 M. Arrowsmith, H. Braunschweig, M. A. Celik, T. Dellermann, R. D. Dewhurst, W. C. Ewing, K. Hammond, T. Kramer, I. Krummenacher, J. Mies, K. Radacki and J. K. Schuster, *Nat. Chem.*, 2016, **8**, 890–894.
11 G. Wang, J. E. Walley, D. A. Dickie, S. Pan, G. Frenking and R. J. Gilliard, *J. Am. Chem. Soc.*, 2020, **142**, 4560–4564.
12 C. Czernetzki, M. Arrowsmith, F. Fantuzzi, A. Gärtner, T. Tröster, I. Krummenacher, F. Schorr and H. Braunschweig, *Angew. Chem., Int. Ed.*, 2021, **60**, 20776–20780.
13 J. T. Boronski, L. R. Thomas-Hargreaves, M. A. Ellwanger, A. E. Crumpton, J. Hicks, D. F. Bekiş, S. Aldridge and M. R. Buchner, *J. Am. Chem. Soc.*, 2023, **145**, 4408–4413.
14 J. T. Boronski, A. E. Crumpton, L. L. Wales and S. Aldridge, *Science*, 2023, **380**, 1147–1149.
15 J. T. Boronski, A. E. Crumpton, A. F. Roper and S. Aldridge, *Nat. Chem.*, 2024, **16**, 1295–1300.
16 C. Berthold, J. Maurer, L. Klerner, S. Harder and M. R. Buchner, *Angew. Chem., Int. Ed.*, 2024, **63**, e202408422.
17 K. G. Pearce, M. S. Hill and M. F. Mahon, *Chem. Commun.*, 2023, **59**, 1453–1456.
18 K. G. Pearce, H.-Y. Liu, S. E. Neale, H. M. Goff, M. F. Mahon, C. L. McMullin and M. S. Hill, *Nat. Commun.*, 2023, **14**, 8147.
19 K. G. Pearce, M. S. Hill and M. F. Mahon, *Organometallics*, 2024, **43**, 432–437.
20 R. Fleischer and D. Stalke, *Inorg. Chem.*, 1997, **36**, 2413–2419.
21 M. Niemeyer and P. P. Power, *Inorg. Chem.*, 1997, **36**, 4688–4696.
22 M. Arrowsmith, M. S. Hill, G. Kociok-Köhn, D. J. MacDougall, M. F. Mahon and I. Mallov, *Inorg. Chem.*, 2012, **51**, 13408–13418.
23 M. Arrowsmith, M. R. Crimmin, M. S. Hill and G. Kociok-Köhn, *Dalton Trans.*, 2013, **42**, 9720–9726.
24 D. Naglav, D. Bläser, C. Wölper and S. Schulz, *Inorg. Chem.*, 2014, **53**, 1241–1249.
25 D. Naglav, B. Tobey, C. Wölper, D. Bläser, G. Jansen and S. Schulz, *Eur. J. Inorg. Chem.*, 2016, 2424–2431.
26 M. Bayram, D. Naglav, C. Wölper and S. Schulz, *Organometallics*, 2016, **35**, 2378–2383.

27 M. Bayram, D. Naglav, C. Wölper and S. Schulz, *Organometallics*, 2017, **36**, 467–473.
28 D. Naglav, B. Tobey, K. Dzialkowski, D. Bäser, C. Wölper, G. Jansen and S. Schulz, *Dalton Trans.*, 2018, **47**, 12511–12515.
29 A. Paparo and C. Jones, *Chem. – Asian J.*, 2019, **14**, 486–490.
30 A. Paparo, C. N. de Bruin-Dickason and C. Jones, *Aust. J. Chem.*, 2020, **73**, 1144–1148.
31 A. Paparo, S. P. Best, K. Yuvaraj and C. Jones, *Organometallics*, 2020, 4208–4213.
32 M. Müller, A. J. Karttunen and M. R. Buchner, *Chem. Sci.*, 2020, **11**, 5414–5422.
33 A. Paparo, A. J. R. Matthews, C. D. Smith, A. J. Edwards, K. Yuvaraj and C. Jones, *Dalton Trans.*, 2021, **50**, 7604–7609.
34 M. R. Buchner and M. Müller, *Dalton Trans.*, 2021, **50**, 7246–7255.
35 C. Berthold, M. Müller, S. I. Ivlev, D. M. Andrada and M. R. Buchner, *Dalton Trans.*, 2023, **52**, 13547–13554.
36 M. R. Buchner, M. Müller and S. S. Rudel, *Angew. Chem., Int. Ed.*, 2017, **56**, 1130–1134.
37 B. Scheibe and M. R. Buchner, *Eur. J. Inorg. Chem.*, 2018, 2300–2308.
38 M. Müller and M. R. Buchner, *Angew. Chem., Int. Ed.*, 2018, **57**, 9180–9184.
39 M. Müller and M. R. Buchner, *Inorg. Chem.*, 2019, **58**, 13276–13284.
40 M. Müller and M. R. Buchner, *Chem. – Eur. J.*, 2020, **26**, 9915–9922.
41 M. R. Buchner, L. R. Thomas-Hargreaves, L. K. Kreuzer, N. Spang and S. I. Ivlev, *Eur. J. Inorg. Chem.*, 2021, 4990–4997.
42 M. R. Buchner, D. Cocic, S. I. Ivlev, N. Spang, M. Müller and R. Puchta, *Dalton Trans.*, 2023, **52**, 5287–5296.
43 D. F. Bekiş, L. R. Thomas-Hargreaves, C. Berthold, S. I. Ivlev and M. R. Buchner, *Z. Naturforsch., B: J. Chem. Sci.*, 2023, **78**, 165–173.
44 M. R. Buchner, L. R. Thomas-Hargreaves, C. Berthold, D. F. Bekiş and S. I. Ivlev, *Chem. – Eur. J.*, 2023, **29**, e202302495.
45 F. Kraus, S. A. Baer, M. R. Buchner and A. J. Karttunen, *Chem. – Eur. J.*, 2012, **18**, 2131–2142.
46 M. Müller and M. R. Buchner, *Chem. Commun.*, 2019, **55**, 13649–13652.
47 H. Bürger, C. Forker and J. Goubeau, *Monatsh. Chem.*, 1965, **96**, 597–601.
48 A. H. Clark and A. Haaland, *Acta Chem. Scand.*, 1970, **24**, 3024–3030.
49 A. H. Clark and A. Haaland, *J. Chem. Soc. D*, 1969, 912–913.
50 D. Naglav, A. Neumann, D. Blaser, C. Wolper, R. Haack, G. Jansen and S. Schulz, *Chem. Commun.*, 2015, **51**, 3889–3891.
51 J. B. Farmer, H. M. M. Shearer, J. D. Sowerby and K. Wade, *J. Chem. Soc., Chem. Commun.*, 1976, 160–161.
52 B. Hall, J. B. Farmer, H. M. M. Shearer, J. D. Sowerby and K. Wade, *J. Chem. Soc., Dalton Trans.*, 1979, 102–109.
53 J. L. Atwood and G. D. Stucky, *J. Am. Chem. Soc.*, 1969, **91**, 4426–4430.
54 M. P. Dressel, S. Nogai, R. J. F. Berger and H. Schmidbaur, *Z. Naturforsch., B: J. Chem. Sci.*, 2003, **58**, 173–182.
55 M. R. Buchner, M. Müller and N. Spang, *Dalton Trans.*, 2020, **49**, 7708–7712.
56 G. E. Coates, F. Glockling and N. D. Huck, *J. Chem. Soc.*, 1952, 4512–4515.
57 G. E. Coates and F. Glockling, *J. Chem. Soc.*, 1954, 22–27.
58 N. A. Bell, G. E. Coates and J. W. Emsley, *J. Chem. Soc. A*, 1966, 49–52.
59 G. E. Coates and M. Tranah, *J. Chem. Soc. A*, 1967, 236–239.
60 N. A. Bell, G. E. Coates and A. H. Fishwick, *J. Organomet. Chem.*, 1980, **198**, 113–120.
61 T. Hohl, T. Sinn and C. Hoch, *Z. Naturforsch., B: J. Chem. Sci.*, 2020, **75**, 509–516.
62 G. Wang, J. E. Walley, D. A. Dickie, A. Molino, D. J. Wilson and R. J. Gilliard, *Angew. Chem., Int. Ed.*, 2021, **60**, 9407–9411.
63 H. Nöth and D. Schlosser, *Inorg. Chem.*, 1983, **22**, 2700–2703.
64 H. Nöth and D. Schlosser, *Chem. Ber.*, 1988, **121**, 1711–1713.
65 L. R. Thomas-Hargreaves, C. Berthold, W. Augustinov, M. Müller, S. I. Ivlev and M. R. Buchner, *Chem. – Eur. J.*, 2022, **28**, e202200851.
66 P. Pyykkö and M. Atsumi, *Chem. – Eur. J.*, 2009, **15**, 186–197.
67 L. R. Thomas-Hargreaves, Y.-Q. Liu, Z.-H. Cui, S. Pan and M. R. Buchner, *J. Comput. Chem.*, 2023, **44**, 397–405.
68 G. Knizia, *J. Chem. Theory Comput.*, 2013, **9**, 4834–4843.
69 Partial charges were calculated with two different programs, IBOViewer and Turbomole. The latter results yielded a more ionic bonding situations in comparison to the results from IBOViewer and the performed Natural Populations Analysis (NPA) as reference. Due to technical problems in IBOViewer with **6**, IAO analysis had to be performed with Turbomole. After adjusting the IBO reference basis set for Be in Turbomole, all results obtained in IBOViewer were reproduced and the IAO analysis for all compounds was performed. The changed parameters and all partial charges are given in the ESI.†
70 P. G. Plieger, K. D. John, T. S. Keizer, T. M. McCleskey, A. K. Burrell and R. L. Martin, *J. Am. Chem. Soc.*, 2004, **126**, 14651–14658.
71 J. K. Buchanan and P. G. Plieger, *Z. Naturforsch., B: J. Chem. Sci.*, 2020, **75**, 459–472.
72 H. Nöth and D. Schlosser, *Eur. J. Inorg. Chem.*, 2003, **2003**, 2245–2254.
73 G. E. Coates and A. H. Fishwick, *J. Chem. Soc. A*, 1967, 1199–1204.
74 L. R. Thomas-Hargreaves, M. Müller, N. Spang, S. I. Ivlev and M. R. Buchner, *Organometallics*, 2021, **40**, 3797–3807.

75 M. R. Buchner and M. Müller, *ACS Chem. Health Saf.*, 2023, **30**, 36–43.
76 J. Elguero and I. Alkorta, *Struct. Chem.*, 2023, **34**, 391–398.
77 M. R. Buchner, *Chem. Commun.*, 2020, **56**, 8895–8907.
78 M. R. Buchner, *Z. Naturforsch., B: J. Chem. Sci.*, 2020, **75**, 405–412.
79 H. Gilman and F. Schulze, *J. Chem. Soc.*, 1927, 2663–2669.
80 D. Naglav, M. R. Buchner, G. Bendt, F. Kraus and S. Schulz, *Angew. Chem., Int. Ed.*, 2016, **55**, 10562–10576.
81 MestReNova, *Mestrelab Research S.L*, Santiago de Compostela, Spain, 2011.
82 *OPUS*, Bruker Optik GmbH, Ettlingen, Germany, 2009.
83 *X-Area*, Stoe & Cie GmbH, Darmstadt, Germany, 2017.
84 *APEX5 Crystallography Software Suite*, Bruker AXS Inc., Madison, WI, USA, 2023.
85 *SADABS/SAINT within APEX5*, Bruker AXS Inc., Madison, WI, USA, 2023.
86 C. B. Hübschle, G. M. Sheldrick and B. Dittrich, *J. Appl. Crystallogr.*, 2011, **44**, 1281–1284.
87 G. M. Sheldrick, *SHELXL-2018/3*, Göttingen, Germany, 2018.
88 G. M. Sheldrick, *SHELXT-2018/2*, Göttingen, Germany, 2018.
89 R. Ahlrichs, M. Bär, M. Häser, H. Horn and C. Kölmel, *Chem. Phys. Lett.*, 1989, **162**, 165–169.
90 *TURBOMOLE V7.7, a Development of University of Karlsruhe and Forschungszentrum Karlsruhe GmbH, 1989–2007*, TURBOMOLE GmbH, since 2007, 2022.
91 C. Adamo and V. Barone, *J. Chem. Phys.*, 1999, **110**, 6158–6170.
92 J. P. Perdew, K. Burke and M. Ernzerhof, *Phys. Rev. Lett.*, 1996, **77**, 3865–3868.
93 F. Weigend and R. Ahlrichs, *Phys. Chem. Chem. Phys.*, 2005, **7**, 3297–3305.
94 A. D. Becke and E. R. Johnson, *J. Chem. Phys.*, 2005, **123**, 154101.
95 S. Grimme, J. Antony, S. Ehrlich and H. Krieg, *J. Chem. Phys.*, 2010, **132**, 154104.
96 S. Grimme, S. Ehrlich and L. Goerigk, *J. Comput. Chem.*, 2011, **32**, 1456–1465.
97 K. Eichkorn, O. Treutler, H. Öhm, M. Häser and R. Ahlrichs, *Chem. Phys. Lett.*, 1995, **240**, 283–290.
98 F. Weigend, *Phys. Chem. Chem. Phys.*, 2002, **4**, 4285–4291.
99 M. Sierka, A. Hogekamp and R. Ahlrichs, *J. Chem. Phys.*, 2003, **118**, 9136–9148.
100 A. E. Reed, R. B. Weinstock and F. Weinhold, *J. Chem. Phys.*, 1985, **83**, 735–746.
101 Chemcraft – Graphical Software for Visualization of Quantum Chemistry Computations. Version 1.8. **https://www.chemcraftprog.com**.